GRAH-RA 77-1414

Second- and third-order piezoelectric stress constants of lithium niobate as determined by the impact-loading technique*

R. A. Graham

Sandia Laboratories, Albuquerque, New Mexico 87115
(Received 19 November 1976; accepted for publication 15 February 1977)

Determination of the e_{22}, e_{33}, and e_{15} second-order piezoelectric stress constants, several third-order piezoelectric stress constants, and the c_{11}^{D} and c_{33}^{D} elastic stiffness constants are reported for lithium niobate from experiments with input strains from 7×10^{-4} to 8×10^{-3} produced by the elastic impact-loading method. Measurements of the e_{33} constant were made on a large number of samples to establish sample uniformity. The differences were found to be less than 1%. The present value of e_{33} is higher than that reported in previous work and appears to call for a revision of the accepted value along with that of the elastic constant c_{33}^{E}. The third-order piezoelectric stress constants are readily detectable, but the values determined in the present investigation are limited in accuracy due to the relatively low strains which could be applied to the samples before conductivity became excessive.

PACS numbers: 77.60.+v, 62.50.+p, 62.20.Dc

I. INTRODUCTION

The purpose of this paper is to report the results of an experimental determination of certain second- and third-order piezoelectric stress constants and several second-order elastic stiffness constants for lithium niobate. The measurements were made with the impact-loading technique.

The piezoelectric properties of lithium niobate are of importance in the operation of a wide variety of piezoelectric devices including transducers, delay lines, filters, and resonators which may operate in either bulk- or surface-wave modes. (For examples of typical devices see Ref. 1.) Although bulk-wave piezoelectric devices are influenced principally by second-order piezoelectric constants, surface-wave devices which operate at microwave frequencies may produce localized strains of the order of 10^{-4} and induce responses influenced by third-order piezoelectric constants. Proposed devices for convolution and correlation of signals at microwave frequencies use the third-order piezoelectric response as the principal mode of operation.[2] Piezoelectric resonators which operate at large fields are also influenced by third-order piezoelectric constants. Furthermore, the determination of third-order elastic constants in piezoelectric solids requires knowledge of the third-order piezoelectric constants.

We have been interested in the use of quartz and lithium niobate piezoelectric gauges[3–5] for precise time-resolved measurements of impulsive loads which produce compressive stresses of the order of 1 GPa (10 kbar) and strains which are typically 10^{-2}. At these large strains output signals may be significantly influenced by nonlinear piezoelectric, dielectric, and elastic response.

Although knowledge of nonlinear piezoelectric constants is of increasing importance, only limited measurements of nonlinear piezoelectric constants have been made and there are no standard techniques for their determination. The first experiment which involved the effect of nonlinear piezoelectric constants was performed by Hruska[6] who detected a change in resonant frequency of quartz resonators as the magnitude of the biasing electric field was increased.

Various techniques which have been used to determine nonlinear piezoelectric constants involve either indirect or direct piezoelectric effects. Those techniques which utilize the indirect effect are (i) strain and/or electric field dependence of ultrasonic-wave velocities or resonant frequencies[7,8] and (ii) pressure derivatives of ultrasonic-wave velocities under different electrical boundary conditions.[9,10] Those techniques which utilize the direct effect are (iii) interaction of microwave-frequency acoustic waves,[11,12] (iv) stress-induced piezoelectric polarization measurements under static loading,[13] (v) strain-induced piezoelectric polarization measurements under impact loading,[14,15] and (vi) pressure-induced hydrostatic piezoelectric polarization measurements under hydrostatic loading.[16] Accuracy of the interpretation of ultrasonic-wave velocity and resonant frequency measurements is hampered by the separation of third-order elastic and piezoelectric contributions, and the most accurate nonlinear piezoelectric constants have been determined with techniques (v) and (vi).

The second-order piezoelectric constants of lithium niobate have been widely investigated; nevertheless, there is a wide variation in the reported values of the d_{33} and e_{33} piezoelectric constants. The most likely explanation for the different values obtained for these constants is a variation in properties due to the effects of ferroelectric domains. The possibility that there are variations in material properties from sample to sample makes it important to determine if present crystal-growth techniques yield crystals with reproducible properties. The impact-loading method is destructive and numerous samples are used; hence, investigation of material reproducibility follows naturally with that technique.

Lithium niobate has been described as a "frozen-in" ferroelectric since the application of an electric field does not rotate in the direction of polarization at tem-

peratures remote from the Curie temperature of 1475 K. The remanent polarization has been found to be unchanged by application of hydrostatic pressure to 2 GPa,[16] but the effect of uniaxial strain on remanent polarization has not been determined.

Section II presents the thermodynamic definitions of material constants which are to be used to interpret the data. In Sec. III the relation between the current pulses from impact-loaded samples and the piezoelectric and dielectric constants is given. The experimental configurations used for the present measurements are then shown in Sec. IV. The results of the measurements are presented in Sec. V and discussed in Sec. VI. Finally, the significance of the present measurements is discussed in Sec. VII.

II. THERMODYNAMIC DEFINITION OF MATERIAL CONSTANTS

Large strains and electric fields are encountered in the present experiments and nonlinear constitutive relations are required for the interpretation of the experimental observations. The formation of nonlinear piezoelectric constitutive relations has been considered by numerous authors,[8,11,17–28] but, as yet, there is no generally accepted notation or definition of terms.

The electrical enthalpy, $H_2 = U - E_j D_j$, is a function of material strain η_{ij}, electric field E_j, and entropy θ. U is the internal energy and D_j is the electrical displacement. The material strain is related to the displacement by the relation[26] $2\,da_j\,da_k\eta_{jk} = dX_i\,dX_i - da_i\,da_i$ where X is the location of a mass element in a spatial coordinate system and a is the location of a mass element in a material coordinate system. The thermodynamic tension t_{ij} is taken to be the derivative of the internal energy with respect to the strain at constant entropy, and the electric displacement D_j is taken to be the derivative of the electrical enthalpy with respect to the electric field at constant entropy and strain. Accordingly, to third-order in energy,

$$t_{ij} = \rho_0\left(\frac{\partial U}{\partial \eta_{ij}}\right) = c^E_{ijkl}\eta_{kl} - e_{kij}E_k + \tfrac{1}{2}C^E_{ijklmn}\eta_{kl}\eta_{mn} - \tfrac{1}{2}f_{klij}E_kE_l - \tfrac{1}{2}e_{ijklm}E_m\eta_{kl} \tag{1a}$$

and

$$D_i = \frac{-\partial H_2}{\partial E_i} = e_{ijk}\eta_{jk} + \epsilon^\eta_{ij}E_j + \tfrac{1}{2}e_{ijklm}\eta_{jk}\eta_{lm} + \tfrac{1}{2}f_{ijkl}E_j\eta_{kl} + \tfrac{1}{2}\epsilon^\eta_{ijk}E_jE_k, \tag{1b}$$

where ρ_0 is the density at zero strain, c^E_{ijkl} is the second-order elastic stiffness constant at constant field, c^E_{ijklmn} is the third-order elastic stiffness constant at constant electric field, e_{kij} is the second-order piezoelectric stress constant, e_{ijklm} is the third-order piezoelectric stress constant, ϵ^η_{ij} is the dielectric permittivity at constant strain, ϵ_{ijk} is the third-order dielectric permittivity, and f_{klij} is the electrostrictive constant. Strains and thermodynamic tensions are taken to be positive in tension. Transformations between thermodynamic tension and stress and between finite strain and compression under uniaxial strain conditions are given in Ref. 14. Small pyroelectric contributions to electric displacement due to isentropic heating are treated in Sec. VI.

Theories which seek solutions in the uncoupled approximation do not include the contributions of piezoelectric stiffening terms in Eq. (1a), while theories which seek solution in the weak-coupling approximation take the uncoupled solutions and add contributions due to the piezoelectric stiffening to account for the electromechanical coupling effects. In the present investigation the data are interpreted in terms of the weak-coupling approximation.

The present investigation was conducted on Z-, Y-, and 36°-rotated—Y-cut (hereafter called the rotated cut) samples. The second-order longitudinal piezoelectric stress constants for the Z- and Y-cut samples are e_{33} and e_{22}, respectively, whereas the rotated cut is characterized by a combination of the four piezoelectric constants. For lithium niobate, a crystal of symmetry $3m$, the rotated linear piezoelectric constant is[29]

$$e'_{22} = 2e_{15}\cos^2\theta\sin\theta + e_{22}\cos^3\theta + e_{33}\sin^3\theta + e_{31}\cos^2\theta\sin\theta, \tag{2}$$

where $\theta = 36°$ for the rotated cut of the present investigation.

Experiments on the Y- and rotated-cut samples involve wave propagation along nonspecific directions in the crystal. When isotropic solids are subjected to a planar impact loading, shock waves propagate through the samples with particle motion directed along the direction of propagation. When anisotropic crystals are subjected to the same loading, this uniaxial strain condition is encountered only if the loading is applied along certain specific directions in the crystal.[30] In the present investigation only the Z-cut samples are loaded along a specific direction. Nevertheless, numerical calculations by Johnson[31] indicate that analysis of the piezoelectric response in terms of uniaxial strain for impact loading along the Y and 36°-rotated—Y directions should be correct to a suitable approximation since the amplitude of the quasi-longitudinal wave is

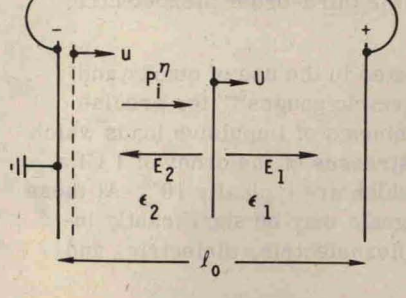

FIG. 1. The electrical conditions in one-dimensional regions of a shock-loaded piezoelectric disk are as shown. The impact was applied to the left face of the disk, and at any time before wave transit time the shock front divides the sample into two characteristic regions within which the conditions are uniform. The electrodes are assumed to be connected with an electrical short circuit. The positive coordinate direction is from left to right.

within 3% of that computed for uniaxial strain conditions.

III. CURRENT PULSES FROM IMPACT-LOADED PIEZOELECTRIC DISKS

In experiments with the impact-loading technique, planar impact loading is applied to large diameter-to-thickness ratio sample disks whose electrodes are arranged in a guard-ring configuration. The impactor is sufficiently thick that stress is maintained at the impact plane for the duration of the experiment. In regions of the disks in which the electric field and motion are uniaxial, the electrical configuration in the quasi-static uncoupled approximation is as depicted in Fig. 1. With the input stress electrode chosen as the reference potential, the current into a low impedance resistive load which acts as an effective short circuit is, in the uncoupled approximation,[14]

$$i=\frac{\alpha(1-u/U)P_i^{\eta}A/t_0}{[(1-u/U)t/t_0+\alpha(1-t/t_0)]^2}\,, \quad 0<t<t_0. \tag{3}$$

In Eq. (3) i is the current in the external circuit connecting the electrodes, α is the ratio of the strained to unstrained permittivity, u is the particle velocity in the region behind the shock front, U is the shock velocity, P_i^{η} is the piezoelectric polarization, A is the area of the change-collecting electrodes, and t_0 is the transit time of the shock front through the thickness of the disk. The time t is taken to be zero upon first application of the load.

In the present model, the electromechanical coupling effects are neglected. Furthermore, it is assumed that $\epsilon_{ijk}^{\eta}E_k$ is negligibly small compared to ϵ_{ij}^{η} and its contribution is ignored. (This assumption has been verified for X-cut quartz.[13]) The electrostrictive effect, manifest as $f_{ijkl}E_j\eta_{kl}$ in Eq. (1b), is treated as a strain-induced change in permittivity and is incorporated into the interpretation of the data through the constant α.

At the time $t=0^+$, the current, called the initial current i_i, is directly related to the piezoelectric polarization by the solution of Eq. (3) for $t=0$,

$$P_i^{\eta}=\alpha t_0[A(1-u/U)]^{-1}i_i, \quad t=0. \tag{4}$$

Thus, measurement of values for i_i and the shock velocity at known input particle velocities provides a direct measure of the piezoelectric polarization if a value can be determined for α. In the uncoupled approximation α may be determined from measurements of i_i and the current at $t=t_0, i_f$. It follows from Eq. (3) that

$$\alpha=[i_f/i_i]^2[1-u/U]^{-1}. \tag{5}$$

Equations (3)–(5) represent solutions for the current in the uncoupled approximation. Before these equations are used to interpret the experimental results the effect of electromechanical coupling must be considered. Solutions for the current in a fully coupled configuration have been given by Lysne[23] and Thurston.[26] A fully coupled solution suitable for numerical evaluation has recently been presented and a computer code has been prepared for performing the calculations.[32] In the following development the solutions of Thurston are modified such that the electromechanical coupling factor in the stressed region is different from that in the unstressed region. The excess current i_c, which is an addition to the current obtained in the uncoupled approximation, is

$$i_c=(b_1+b_2)\int_0^t i(t)\,dt, \tag{6}$$

where $i(t)$ is the total current, $b_1=k_0^2B_1/t_0$, $b_2=\tilde{k}^2B_2/t_0$, k_0^2 is the electromechanical coupling factor computed to represent the effects in the unstrained region, $\tilde{k}^2$ is the electromechanical coupling factor computed to represent the effects in the strained region, and B_1 and B_2 are the acoustic impedance ratios $(1+Z_1/Z)^{-1}$ and $(1+Z_2/Z)^{-1}$ for the unstrained and strained regions, respectively, where Z is the acoustic impedance of the sample and Z_1 and Z_2 are acoustic impedances of the material in contact with the input and back electrodes, respectively.

It can be observed from Eq. (6) that the excess current due to electromechanical coupling is initially zero then changes smoothly in time. For a step-function current pulse the extra current increases linearly in time. The magnitude of the increase is directly dependent on the impedance of the materials in contact with the electrodes of the piezoelectric sample and the electromechanical coupling coefficient of the piezoelectric sample.

The theory presented in this section is applied to the determination of second- and third-order piezoelectric constants by computing the piezoelectric current from Eq. (4) for a series of experiments at different strains. The piezoelectric polarization is identified as the strain-induced contributions to displacement in Eq. (1b), and the polarization versus strain data are fit by the polynomial relation $P_i^{\eta}=e_{ij}\eta_j+\frac{1}{2}e_{ijk}\eta_j\eta_k$, where the abbreviated notation is applied.

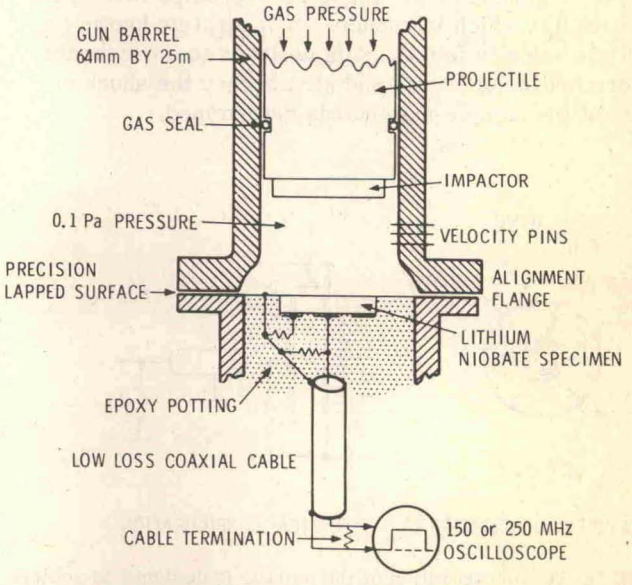

FIG. 2. The impact-loading experiment is illustrated schematically in this figure. Loading of the sample is accomplished by the precisely aligned impact of the impactor upon the sample. The current pulse from the sample is measured in a low impedance resistive circuit as the shock wave propagates through the sample.

IV. EXPERIMENTAL ARRANGEMENT

The impact-loading technique for determining piezoelectric stress constants has been described in previous papers,[3,14,33] and, except for differences in detail, the present investigation follows the prior procedures.

A schematic of the impact-loading arrangement and the instrumentation is shown in Fig. 2. An impacting material whose mechanical properties have been accurately characterized was attached to the impact face of a projectile which was accelerated to a preselected velocity in a smooth-bore compressed gas gun and impacted upon the sample. Immediately prior to impact the velocity of the impactor was measured to an accuracy of $\pm 0.1\%$. The alignment between the impacting surfaces was precisely controlled such that the median value of the "tilt" or angular misalignment for the present measurements was 300 μrad.

In the present experiments most of the measurements were taken with impact velocities of from 20 to 100 m/s. In order to routinely achieve preselected velocities in this unusually low-velocity range, the gas gun[34] was modified so that the projectile could be muzzle loaded and the initial location of the projectile set at distances of from 1 to 3 m from the specimen depending upon the desired impact velocity.

The samples were loaded over large planar areas, but observations of electrical responses were limited to a central region of the sample to ensure that all measurements were taken under uniaxial strain conditions. Under these uniaxial strain conditions the conservation of mass and momentum relations lead to the expressions $S=u/U$ and $T=\rho_0 Uu$, respectively, where S is the strain and T is the component of stress in the propagation direction. (The transformation between η and S, and t and T for uniaxial strain is given in Ref. 14.) It is apparent from these relationships that an impact loading which introduces an accurately known particle velocity into the sample leads to an accurate determination of stress and strain when the shock velocity of the sample material is determined.

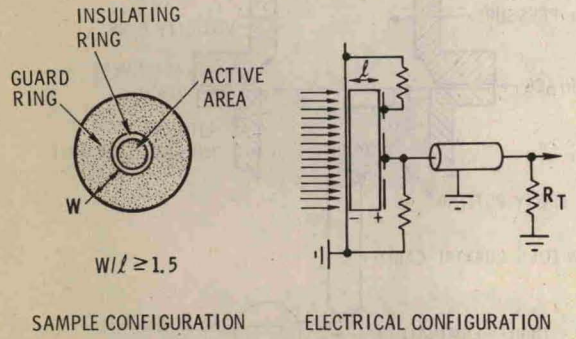

FIG. 3. The configuration of the sample is designed to achieve one-dimensional strain and electric field conditions in the active area of the sample. The electrical configuration is a simple resistive circuit with a terminated low-loss coaxial cable transmission system. R_T is the termination resistor. The sample polarity indicated is that determined with the sample in compression.

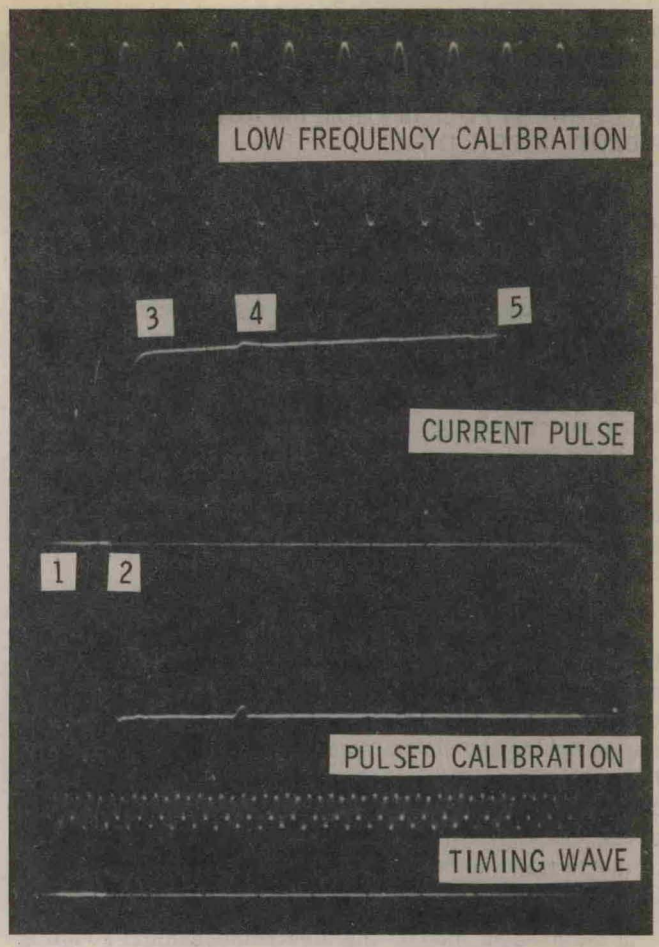

FIG. 4. Typical current pulse obtained on Z-cut lithium niobate. The current pulse is in the center of the record. Time increases from left to right. At 1 the oscilloscope is triggered. Impact begins at 2 and is complete at 3. The small perturbation at 4 is a reflection from the input termination which travels down the signal cable and back to the input. The shock wave arrives at the rear electrode at 5. The current pulse duration is 360 ns. The pulse amplitude is about 2 A from a sample with an area of 8×10^{-5} m^2 and a thickness of 2.6 mm. The impact stress is 1.2 GPa which corresponds to a strain of 4.9×10^{-3}.

Under planar impact conditions the particle velocity u, imparted to the sample by the impact, is

$$u=[(Z_I)/(Z_s+Z_I)]u_0, \tag{7}$$

where u_0 is the impact velocity, $Z_s=\rho_0 U$, the mechanical impedance of the sample at the particle velocity of the experiment, ρ_0 is the initial density, and U is the shock velocity of the sample material; similarly, Z_I is the mechanical impedance of the impactor. In the present experiments the impactors were X-cut quartz,[14] polymethyl methacrylate (PMMA),[35] or Z-cut lithium niobate.

As the shock wave propagates through the sample, an electric current is produced in an external low-impedance resistive circuit. As indicated by Eq. (3), this current pulse is approximately rectangular in shape with a pulse duration controlled by the time required for the shock wave to propagate through the thickness of the sample. In the various experiments this transit time is approximately 360—860 ns.

The sample and electrical configuration is shown in Fig. 3. One-dimensional electrical conditions within the active volume of the sample are achieved by a guard-ring configuration which restricts the region of observation to the central portion of the disk. Due to the symmetry of the strain-induced polarization and the electric fields, the active charge-collecting area extends to a diameter located at the center of the insulating ring. The resistive loads were varied in the range from about 3 to 15 Ω from experiment to experiment to keep the output voltage approximately equal to the 6.54-V calibration pulse.[33] Most of the samples were oriented such that the shock propagated from the grounded negative-polarity electrode to the positive-polarity electrode.

Experiments from which data on piezoelectric constants were obtained were conducted on 27 Z-cut samples, 15 Y-cut samples, and 6 36°-rotated—Y-cut samples. Data on Z-cut samples were obtained from samples cut from 9 different single-crystal boules. Other experiments whose detailed results are to be reported elsewhere were conducted to study the shock-induced conductivity which is, in many respects, similar to that observed in X-cut quartz.[36,37]

Experiments were also conducted to determine the Hugoniot elastic limit and wave speed in the Z-cut samples. These experiments were conducted with the quartz gauge "front-back" configuration[33] in which the impact load is applied and measured by an impacting quartz gauge. The propagated wave profile is also monitored by a quartz gauge, which provides an accurate time-resolved measure of the wave profile from which the Hugoniot elastic limit can be determined. Front-back configuration experiments were also conducted below the elastic limit to determine the shock velocity to an accuracy of $\pm\frac{1}{2}\%$. Wave transit time measurements obtained from the durations of the current pulses give velocity to an accuracy of $\pm 1\%$.

Most of the material was a selected "transducer grade"; however, three optical-grade Z-cut samples were also investigated. The optical-grade material has very low residual strain and fewer light-scattering centers but is only available in diameters up to 12.5 mm. Our transducer-grade material was selected by optical inspection to avoid samples with large internal strains. The crystals were free of cracks of bubbles when viewed by a high-intensity lamp; inclusions were less than $1/\text{cm}^3$. The crystals were clean, pale yellow, single domain, and twin free.

The samples were right-circular-cylindrical disks of various diameters and thicknesses. Early in the investigation diameters of the Z-cut samples were typically 19 mm and thicknesses were 2.5 mm. Specimens of optical-grade material were typically 12.5 mm in diameter and 2.5 mm in thickness. The first Y-cut samples were 25 mm in diameter and 2.5 mm thick. Later in the investigation larger crystals became available and Z- and Y-cut samples 33 mm in diameter and 6.3 mm in thickness were used. All the 36°-rotated—Y-cut samples were of this larger size. In general, the large-diameter samples contained larger residual strains. All samples were grown and poled by Crystal Technology, Inc., and the disks were x-ray oriented within 1° and fabricated by either Crystal Technology, Inc. or Specialty Engineering Associates.

V. RESULTS

A typical current pulse obtained from an experiment on a Z-cut sample (Fig. 4) is characterized by a jump in current while the stress is being applied over the entire active area followed by a slow increase in current with time. The magnitudes of the increases in current with time are similar for Z-cut lithium niobate and X-cut quartz,[14] but solutions for the current from Eqs. (3) and (6) show that, while the increase in current for quartz is dominated by the effect of the strain u/U, the increase in current for lithium niobate is dominated by the electromechanical coupling effects. A value of $\alpha = 1.00$ was used in Eq. (4) to compute the piezoelectric polarization from the initial current jump since, within the reproducibility of the data, there was no discernible change in the magnitude of the increase in current with time as the input strain was changed.

The increase in current during the shock-wave transit time for the Y- and 36°-rotated—Y-cut samples amounted to about 50% of the initial value for the quartz impactor experiments due to the electromechanical coupling effect.

The theory used to interpret the current pulses presumes that the sample is elastic and that the conductivity is zero. Hugoniot elastic limit measurements for the Z-cut samples indicated a peak stress of 2.5 GPa which relaxed in time to a stress of 1.9 GPa. Relatively low shock-induced conductivity thresholds significantly limited the maximum strains which could be used in the experiments.

Detailed tabulation of the experimental results for Z-cut lithium niobate is given in Table I. It is notable that the strains and particle velocities in the present investigation are, by far, the lowest achieved in shock-loading experiments in which active measurements are taken. The lowest strain of 7×10^{-4} overlaps the maximum strains obtained in the static high-pressure ultrasonic measurements and those achieved in surface acoustic waves at microwave frequencies.

In the tabulation it is relatively easy to note the extent of the electromechanical coupling from the tabulated values of i_f/i_i. The larger values obtained when using the PMMA impactors (prefix P on Shot No.) are as expected from solutions of Eq. (6).

In a number of cases a slight conductivity effect is noted, but the effect is not sufficient to cause an error in computation of the piezoelectric polarization from the observed initial current.

Results of the experiments on Y- and 36°-rotated—Y-cut samples are shown in Tables II and III, respectively.

A more detailed plot of the results from individual experiments is shown for the three orientations in Fig. 5. The data on Z-cut lithium niobate were obtained under a wide range of conditions which are indicated in the symbols. It is apparent that the responses of the

TABLE I. Summary of experimental results—Z-cut samples. u_0 is the impact velocity, u is the particle velocity, T is the longitudinal component of stress, η is the material strain, i_i is the initial current jump, i_f is the current at wave transit time, l is the specimen thickness, A is the charge-collecting area computed from a diameter to the center of the insulating ring, U is the shock velocity, P_i^η is the piezoelectric polarization computed from Eq. (3), and k is the piezoelectric current coefficient computed from $k = i_i l/TAU$. $U = 7.33$ km/s, $\rho_0 = 4.64$ Mg/m^3, and $\alpha = 1.00$.

Shot No.[a]	u_0 (m/s)	u (m/s)	T (GPa)	$S = u/U$ ($\times 10^{-4}$)	$-\eta$[b] ($\times 10^{-4}$)	$i_i l/AU$ (mC/m^2)	i_f/i_i	P_3^η (mC/m^2)	k[c] (mC/m^2 GPa)	Remarks
P-1101	56.28	5.234	0.178	7.14	7.14	1.31	1.08	1.31	7.35	
Q-868	20.79	6.40	0.218	8.74	8.73	1.56	• • •	1.56	7.16	
P-1105	100.5	9.56	0.325	13.0	13.0	2.40	1.11	2.40	7.38	
Q-1100	32.23	9.93	0.338	13.54	13.53	2.46	• • •	2.46	7.27	Nonlinear current ramp
Q-853	35.71	11.00	0.374	15.01	15.00	2.66	• • •	2.66	7.11	
Q-1102	37.42	11.52	0.392	15.72	15.71	2.90	1.07	2.90	7.40	
Q-857	43.56	13.41	0.456	18.30	18.28	3.31	1.06	3.32	7.26	
Q-1010-N	55.86	17.20	0.585	23.47	23.44	4.39	1.05	4.40	7.50	Negative polarity
Q-1024-O	57.27	17.64	0.600	24.07	24.04	4.50	1.07	4.51	7.50	Optical grade
Q-1009-N	63.00	19.40	0.660	26.47	26.43	4.86	• • •	4.88	7.36	Negative polarity
Q-883	64.76	19.95	0.678	27.21	27.17	4.98	• • •	4.99	7.35	
Q-1017	67.84	20.90	0.711	28.51	28.47	5.33	1.06	5.34	7.50	
Q-1015-N	68.79	21.19	0.721	28.91	28.87	5.31	1.06	5.33	7.36	Negative polarity
Q-848	75.70	23.31	0.793	31.81	31.76	5.98	• • •	6.00	7.54	
L-1119	49.07	24.54	0.835	33.47	33.41	6.16	• • •	6.18		Symmetric impact, slight conductivity
Q-1032-O	83.59	25.74	0.875	35.12	35.06	6.58	1.07	6.60	7.52	
Q-858	88.04	27.12	0.922	36.99	36.92	6.89	1.07	6.92	7.47	
Q-914	93.00	28.64	0.974	39.07	38.99	7.23	1.06	7.26	7.42	
Q-1062	100.4	30.91	1.051	42.17	42.08	7.87	• • •	7.90	7.49	Slight conductivity
Q-1016-N	100.9	31.07	1.057	42.38	42.29	7.78	• • •	7.82	7.36	Negative polarity, slight conductivity
Q-1023-O	102.0	31.42	1.068	42.87	42.78	7.93	1.08	7.96	7.43	Optical grade
Q-851	109.6	33.76	1.148	46.05	45.94	8.50	• • •	8.54	7.40	Slight conductivity
Q-881	112.1	34.52	1.174	47.09	46.98	8.81	1.08	8.86	7.50	
Q-937	116.8	35.98	1.224	49.08	48.96	9.02	1.10	9.06	7.37	
Q-939	121.7	37.49	1.275	51.15	51.02	9.50	• • •	9.55	7.45	Slight conductivity
Q-938	126.1	38.84	1.321	52.98	52.84	9.86	• • •	9.91	7.46	Slight conductivity
Q-909	136.8	42.13	1.433	57.48	57.31	10.85	• • •	10.91	7.57	Slight conductivity

[a] The prefix on the Shot No. indicates Q for an X-cut quartz impactor, L for a Z-cut lithium niobate impactor, and P for a PMMA impactor. The suffix O indicates an optical-grade sample and the suffix N indicates a negative-polarity orientation in which the shock front propagates from the positive to the negative electrode. Shot numbers are chronological and numbers greater than 1060 indicate experiments on 32-mm-diam samples.

[b] $\eta = S(\frac{1}{2}S - 1)$. See Ref. 14.

[c] The fit to the k-vs-stress data is $k = [7.26 \pm 0.044 + (0.18 \pm \pm 0.05)T]$ mC/m^2 GPa, standard deviation = 0.092.

optical-grade and transducer-grade materials were the same. The data also indicate that there is no difference in the response of negative orientation samples for which the shock propagation direction is reversed relative to the direction of the spontaneous polarization.

The Y-cut data in Fig. 5 show that the nonlinear constant is of opposite sign to that observed for Z-cut

TABLE II. Summary of experimental results—Y-cut samples. $U = 6.88$ km/s, $\rho_0 = 4.64$ Mg/m^3, and $\alpha = 1.00$. Notation is the same as that used in Table I.

Shot No.[a]	u_0 (m/s)	u (m/s)	T (GPa)	$S = u/U$ ($\times 10^{-4}$)	$-\eta$ ($\times 10^{-4}$)	$i_i l/AU$ (mC/m^2	i_f/i_i	P_2^η (mC/m^2)	k[b]
P-1103	56.73	5.482	0.175	7.969	7.937	1.83	1.77	1.83	10.47
Q-1087	27.87	8.974	0.286	13.04	13.03	3.11	1.53	3.11	10.87
P-1104	96.37	9.67	0.309	14.06	14.05	3.19	1.65	3.20	10.33
Q-1064	39.13	12.60	0.402	18.31	18.29	4.63	• • •	4.64	11.52
Q-1088	39.80	12.81	0.409	18.62	18.60	4.39	1.53	4.40	10.73
Q-1056	47.24	15.21	0.486	22.11	22.09	5.27	• • •	5.28	10.84
Q-1089	60.56	19.50	0.622	28.32	28.30	6.56	1.57	6.58	10.54
Q-1067	67.94	21.88	0.698	31.80	31.75	7.69	1.49	7.71	11.02
Q-1055	82.37	26.52	0.847	38.55	38.48	8.72	• • •	8.78	10.30
Q-1054	90.04	28.99	0.925	42.14	42.05	9.70	1.46	9.73	10.48
Q-1098	100.1	32.24	1.029	46.86	46.75	10.65	1.53	10.70	10.35
Q-1053	120.2	38.70	1.235	56.26	56.10	12.75	1.45	12.82	10.32
Q-1094	146.4	47.12	1.504	68.50	68.27	15.64	1.53	15.75	10.40
Q-1066	161.1	51.87	1.66	75.40	75.12	17.24	1.52	17.37	10.39
Q-1096	166.1	53.47	1.71	77.72	77.42	17.69	1.50	17.83	10.35
Q-1099	175.7	56.54	...	82.19	81.85	18.43	...	18.58	10.24

[a] Shot numbers greater than 1085 indicate experiments on 32-mm-diam samples.

[b] The fit to the k-vs-stress data is $k = [10.9 \pm 0.14 - (0.34 \pm 0.14)T]$ mC/m^2 GPa, standard deviation = 0.30.

TABLE III. Summary of experimental results—36°-rotated Y-cut samples. $U = 7.33$ km/s, $\rho_0 = 4.64$ Mg/m^3, and $\alpha = 1.00$. Notation is the same as that used in Table I.

Shot No.	u_0 (m/s)	u (m/s)	T (GPa)	u/U ($\times 10^{-4}$)	$-\eta$ ($\times 10^{-4}$)	$i_i l/AU$ (mC/m^2)	i_f/i_i	P_3^η (mC/m^2)	k [a]
P-1107	68.01	6.35	0.216	8.66	8.66	3.96	1.50	3.97	18.35
P-1106	108.0	10.32	0.351	14.1	14.07	6.59	1.94	6.50	18.77
Q-1091	36.48	11.24	0.382	15.33	15.32	7.166	1.45	7.177	18.75
Q-1095	58.84	18.12	0.616	24.72	24.69	11.43	1.50	11.46	18.57
Q-1092	61.63	18.98	0.646	25.90	25.87	12.09	1.42	12.12	18.72
Q-1093	71.30	21.96	0.747	29.96	29.92	13.94	1.48	13.98	18.66

[a] The fit to the k-vs-stress data is $k = 18.64$ in C/m^2 GPa, standard deviation = 0.16.

lithium niobate. The scatter in the Y-cut data is probably the result of the combined effect of tilt, which prevents a reading at $t = t_0$ and the large electromechanical coupling effect affecting the observed value of the initial current. There is no discernible nonlinear effect in the data for the 36°-rotated—Y-cut samples.

The shock velocity determined from either the current pulse duration measurements or from the quartz gauge impact and propagated wave profile measurements are shown in Table IV. Given the experimental accuracy of ± 1 and $\pm \frac{1}{2}\%$, respectively, for the two techniques and the small strains of the experiment, no change in wave speed with strain was detected. The data of Table IV generally indicate ranges which are within the experimental accuracies. There is good agreement between the two independent techniques used to measure the shock velocity of the Z-cut samples.

VI. DISCUSSION OF RESULTS

Material constants and effects observed in the present investigation which are to be discussed and compared to prior work include second- and third-order piezoelectric stress constants, second-order elastic constants as determined from the shock velocity, electromechanical coupling effects on the current pulse, and thresholds for shock-induced conductivity.

A. Piezoelectric stress constants

The second- and third-order piezoelectric constants derived from least-squares polynomial fits to the piezoelectric polarization versus strain data are summarized in Table V and compared to prior work on quartz with the same technique. The experimental error in the determination of the e_{33} constant is about 2%. There is a possible error of 3% in the analysis of the Y- and rotated-cut data because of the interpretation based on uniaxial strain.

In spite of the large number of samples, crystal boules and grades, the precision indicated by the standard error of from 0.9 to 1.5% can be fully accounted for by the precision of the measurement technique. This observation indicates that the material constants are reproducible from sample to sample to a degree which is small compared to the standard errors. Another indication of the reproducibility of the material constants comes from the observation that the present piezoelectric constants differ only slightly from earlier reports of this same investigation when less complete data were available.[4,15,25]

The present observation of the reproducibility of material constants is in agreement with similar conclusions drawn from measurements of the linear and nonlinear hydrostatic piezoelectric constants[16] and data in the Appendix. It appears that the present techniques for crystal growth, poling, and quality control to select

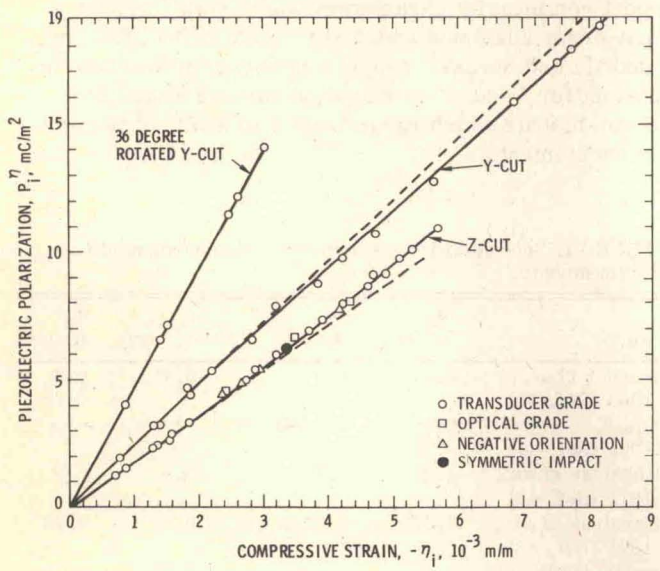

FIG. 5. Piezoelectric polarization versus strain for the three crystallographic orientations of lithium niobate investiaged in the present investigation. The unusually low strains achieved in the present investigation compared to conventional impact-loading experiments are of particular interest. The dashed lines are extrapolations of the linear behavior observed at small strains.

TABLE IV. Shock velocity measurements.

Experiment [a]	U (km/s)	Standard deviation (km/s)	Range (km/s)	No. observations
Z-cut A	7.33	0.038	-0.05 $+0.07$	26
Z-cut B	7.32	0.030	± 0.03	3
Y-cut A	6.90	0.038	± 0.06	10
Rotated cut A	7.35	0.057	± 0.07	6

[a] "A" series of experiments determined shock velocity from sample thickness and current pulse duration. "B" series experiments determined shock velocity from sample thickness and quartz gauge measurements of the time difference between impact and wave arrival at rear surface.

TABLE V. Second- and third-order piezoelectric stress constants of lithium niobate and quartz. It is conventional to assign a positive sign to the longitudinal second-order piezoelectric constants and in this tabulation we have followed that practice. Since strains are normally considered positive in tension, the signs of the third-order constants are assigned on that basis.

Sample Lithium niobate	e_{ij} (C/m^2)	e_{ijk} (C/m^2)	e_{ijk}/e_{ij} (C/m^2)
$i=j=k=3$	1.80 ± 0.016	-21 ± 7	-11
$i=j=k=2$	2.37 ± 0.036	21 ± 10	$+9$
$i=1, j=5$	3.83[a]	• • •	• • •
Rotated cut	4.65 ± 0.053	0	• • •
Quartz			
$i=j=k=1$	0.171 ± 0.0009	-2.62 ± 0.05	-15.3

[a] A value of the e_{15} constant is derived from the fit to the rotated-cut data by solution of Eq. (2). The e_{22} and e_{15} constants determined from the present investigation were used in the calculation with the e_{31} constant determined by Smith and Welsh (Ref. 39). Since the e_{31} constant is relatively small, the calculated e_{15} constant is not sensitive to the value chosen for e_{31}.

transducer-grade lithium niobate yields samples with material constants which are reproducible to a precision of substantially less than 1%.

Although the conclusion on the reproducibility of material constants is drawn from observations of the second-order piezoelectric constants, it should be observed that the reproducibility extends to the elastic constants as well. The current measurement from which the piezoelectric constants are derived is directly dependent on the elastic constants through the dependence of the current on shock velocity. Sample-to-sample variations in the shock velocity would cause corresponding variations in the current and affect the precision of the measurements.

The present value of e_{33} is sufficiently accurate to justify making a correction for the change in polarization caused by adiabatic heating and the pyroelectric effect. For the relatively small compressions of the present experiments, the compression is adiabatic and the increase in temperature ΔT is

$$\Delta T = [(V_0/V)^{\Gamma} - 1]T_0, \tag{8}$$

where T_0 is the initial temperature, V_0 is the initial volume, V is the compressed volume, and Γ is the Grüneisen coefficient. For small compressions $\Delta T = \Gamma S T_0$, where $S = 1 - (V_0/V)$, and the resulting pyroelectric polarization per unit strain is $(\partial P^S/\partial S^T) = \Gamma T_0 \tau$, where P^S is the spontaneous polarization and τ is the *primary* pyroelectric constant. In the present experiments $\Gamma = 1.38$ and $\tau = 5.0 \times 10^{-5}$ C/m^2 K, and it is found that $(\partial P^S/\partial S^T) = 2.07 \times 10^{-2}$ C/m^2 which is 1.2% of e_{33}.[38] The e_{33} reported in Table V has been corrected for the pyroelectric contribution. From symmetry considerations it is known that there is no effect on e_{22} and the effect is negligible for the rotated cut.

The e_{22} and e_{15} values reported by the various investigators and summarized in Table VI show a standard deviation of about 2%, whereas the e_{33} values (as well as those for d_{33}, which is not tabulated) show a standard deviation of 12%. This poor reproducibility of values for e_{33} is probably a result of material reproducibility problems in crystals utilized in earlier investigations. The present investigation included examination of material reproducibility in some detail and provides a direct measure of e_{33} with well-defined errors, and the present value of e_{33} is significantly greater than reported in prior work. Recent measurements of the hydrostatic piezoelectric constant,[16] which is the sum of d_{33} and $2d_{31}$, indicated that d_{33} is also significantly greater than that reported in prior work.

The third-order piezoelectric stress constants determined in the present investigation are shown in Table V and compared to previous measurements on X-cut quartz. The errors of the present third-order constants are large since higher-order piezoelectric contributions are small relative to the second-order contribution. Nevertheless, the third-order contributions are readily apparent and well defined, and the errors of the present work are less than has been achieved with other techniques. The higher-order constant of the Y-cut material is particularly interesting since the sign is positive compared to the negative sign observed on Z-cut lithium niobate and X-cut quartz.

The only direct comparison of the present measurements to other work comes from the work of Korobov and Lyamov[8] who gave order-of-magnitude estimates for various third-order constants of lithium niobate. Their estimate of 10 C/m^2 for e_{333} is about a factor of 2 smaller than the present value. For other third-order constants in lithium niobate, Korobov and Lyamov[8] give order-of-magnitude estimates for the various constants which range from -3 to 190 C/m^2. From static electric field dependencies of acoustic resonances in lithium niobate, Thompson and Quate[2] report nonlinearity parameters which yield various third-order constants which vary from 12 to 150 C/m^2. Luukkala and Suraka[11] report a nonlinear piezoelectric constant for Y-cut Z-propagating surface waves in lithium niobate which range from 8 to 22 C/m^2 in various experiments.

TABLE VI. Second-order piezoelectric stress constants of lithium niobate.

Author	e_{22} (C/m^2)	e_{33} (C/m^2)	e_{15} (C/m^2)	e_{31} (C/m^2)
Warner *et al.*, 1966 (Ref. 40)	2.5	1.3	3.7	0.2
Smith, 1971 (Ref. 41)	• • •	1.62—1.78	• • •	• • •
Chkalova *et al.*, 1971 (Ref. 42)	2.5	1.7	3.8	• • •
Korolyuk *et al.*, 1971 (Ref. 43)	2.52	1.67 (1.72)	3.60	0.75
Smith and Welsh 1971 (Ref. 39)	2.43	1.33	3.76	0.23
Graham, 1973 (Ref. 15)	• • •	1.78[a]	• • •	• • •
Nakagawa *et al.*, 1973 (Ref. 24)	2.5	1.42	3.8	0.35
Present work	2.37	1.80[a]	3.83	• • •

[a] Corrected for a pyroelectric contribution of 1.2%.

TABLE VII. Longitudinal elastic constants of lithium niobate. ± indicates standard deviation. Units are 10^{11} N/m^2.

Author	c_{33}^D	c_{33}^E	c_{11}^D	c_{11}^E
Warner *et al.*, 1967 (Ref. 40)	2.52	2.45	2.19	2.03
Korolyuk *et al.*, 1971 (Ref. 43)	2.51	2.40	2.18	2.02
Chkalova *et al.*, 1974 (Ref. 42)	2.51	2.38		1.99
Smith and Welsh, 1971 (Ref. 39)	2.495	2.424	2.198	2.030
Nakagawa *et al.*, 1973 (Ref. 24)	2.51	2.43	2.15	2.0
Present work	2.49 ± 0.028	2.36 ± 0.028 [a]	2.21	2.06 ± 0.03 [a]

[a] Calculated from $c_{ii}^E = c_{ii}^D - (e_{ii}^2 \epsilon_{ii}^T)/C_{ii}^E$) with c_{ii}^D and e_{ii} as determined from the present work.

B. Shock velocity measurements—Second-order elastic constants

In the present experiments the strains are too small to invoke detectable third-order contributions to wave speed; however, the data are sufficient to determine piezoelectrically stiffened and unstiffened second-order elastic constants.

In the present experimental configuration, in which the electrodes are connected with an effective short circuit, the propagation of the shock wave through the samples is characterized by a jump in strain and an accompanying jump in electric field, each of which is constant in time to a very close approximation (see solutions for the electric fields in Ref. 37). The velocity of the shock wave is

$$\rho_0 U^2 = [T]/[S], \tag{9}$$

where ρ_0 is the initial density, U is the shock velocity, and [ ] indicates a jump in the variable across the shock. Based on a constitutive relation such as Eq. (1a), the jump in stress for fixed jump in strain has components of the unstiffened elastic constant c^E and the jump in electric field which invokes the piezoelectric stiffening. For a constant jump in electric field the wave speed is constant with a magnitude equal to the piezoelectrically stiffened elastic constant c^D, the constant determined at constant electric displacement. Thus, the shock velocity measurements of the present investigation provide a direct measure of the piezoelectrically stiffened elastic constants. {The same conclusion follows from considering a constitutive relation of the form $T = \hat{T}(S, D)$ for the case $[D] = 0$.}

In prior work on X-cut quartz[14] the shock velocity measurements could not distinguish between piezoelectrically stiffened and unstiffened wave velocities since the electromechanical coupling is small, such that the velocities differ by only $\frac{1}{2}\%$. For lithium niobate, however, the coupling is larger and the stiffening effect is readily apparent. The shock velocity measurements of the present investigation reported in Table IV are in excellent agreement with the ultrasonic wave speeds reported by Smith and Welsh[39] which are determined more accurately than in the present work.

The elastic stiffness constants derived from the present investigation are shown in Table VII and compared to previous work. The agreement between our c_{33}^D elastic stiffness with that observed by Smith and Welsh indicates that the larger e_{33} constant of the present work leads to a lower computed value for c_{33}^E than that reported by Smith and Welsh.[39]

It should be emphasized that even though the shock velocity measurements of the present work are not as precise as those obtained ultrasonically, the piezoelectric constants observed in the present work are independent of the shock velocity measurements since both the computed piezoelectric polarization and the strain are inversely proportional to the shock velocity.

C. Electromechanical coupling effect on the current pulses

As indicated in Eq. (6), the current pulse deviates from that predicted from the uncoupled solution, Eq. (3), by a time-dependent factor which depends on the electromechanical coupling factor and the acoustic impedance of the materials in contact with the front and back electrodes. This excess current due to electromechanical coupling is indicated by the i_f/i_i column in Table I.

Based on Eq. (6) and a model in which the back electrode is in contact with epoxy, the predicted ratio of final current i_f to initial current i_i is 8.9% for the quartz impactor experiments and 10.0% for the PMMA impactor experiments. The experimentally observed values are 7 ± 1.6 and 10 ± 1.4%, respectively (± indicates standard deviation). The difference between predicted and observed excess current and the scatter observed from experiment to experiment is most likely due to the solder connection to the back electrode which is not of insignificant size and may vary from experiment to experiment.

The excess current observed in the 36°-rotated experiments with the quartz impactors was 46 ± 3.5% compared to a predicted value of 58%. This observed excess current is lower than the predicted value as was the case for the Z-cut samples. For the PMMA impactors, one experiment gave an anomalously large excess current while the other experiment was lower than the predicted value of 66%.

The most unusual and as yet not fully explained observation of the present investigation is the large excess current, 51 ± 3.6%, observed in the Y-cut quartz impactor experiments compared to the computed value of 11% based on the uniaxial longitudinal piezoelectric constant e_{22}. The much larger than expected excess

current apparently indicates that the electromechanical effects resulting from conditions at the electrodes involve a substantial shear contribution which is not accounted for in the planar uniaxial strain models.

D. Threshold for shock-induced conductivity

Shock-induced conductivity observed in X-cut quartz has been found to be a consequence of stress-induced dielectric breakdown at the relatively large electric fields, about 10^8 V/m, produced by the piezoelectric effect.[36,44] Two factors, sample size and crystallographic orientation, affected the observed thresholds for shock-induced conductivity. Furthermore, the magnitudes of the residual strains within the samples were observed to affect the magnitude of the conductivity.

For Z-cut lithium niobate the threshold for conductivity varied from about 0.8 GPa for the thick samples to about 1.2 GPa for the thin samples. These stresses correspond to electric fields of 2.4×10^7 and 4.4×10^7 V/m, respectively. Whether this thickness dependence is a result of time delays for the initiation of breakdown[5] or lower residual strains in the thin samples which were obtained from smaller-diameter boules is not known.

In a special series of experiments samples were obtained with unusually large internal strain, with normal internal strain, and with unusually low internal strain. Although the thresholds for shock-induced conductivity were not significantly affected by the degree of internal strain, the magnitude of the conductivity was greater for the highly strained material.

The thresholds for shock-induced conductivity for the rotated-cut samples, which were all thick, were 0.8 GPa and a corresponding electric field of 6×10^7 V/m.

The threshold for conductivity in thick Y-cut samples was 1.8 GPa. Thus, this particular orientation has a much higher threshold than the other orientations. It is not known whether the higher threshold for the Y-cut samples is due to improved material quality or due to inherent material properties.

The physical basis for the observed shock-induced conductivity and its dependence on sample size, internal strain, and crystallographic orientation is an important area for further study.

VII. CLOSURE

The present investigation has determined three of the four second-order piezoelectric stress constants and two third-order piezoelectric stress constants of lithium niobate. Even though prior work has shown a variation of ±15% in the value of the e_{33} constant, the present work demonstrates that material constants of presently available crystals are reproducible to an accuracy of less than 1%. The present value of the e_{33} constant apparently calls for a downward revision of the c_{33}^E constant of lithium niobate.

There is no evidence for a change in remanent polarization with strain. The observed sample responses appear to be fully explained by the piezoelectric effect. The present measurements further demonstrate the utility of the impact-loading technique for determination of second- and third-order piezoelectric stress constants. Although this technique has provided the most accurate third-order constant measurements of any technique used to date, it is limited in application since a successful investigation requires a significant number of crystals with diameters of 1 cm or greater and the property of high resistivity at elastic strains of a few percent. In the present investigation the accuracy of the third-order constant measurement is relatively large since the maximum strains were limited to about 7×10^{-3}.

It is worthy to note that lithium niobate is the only piezoelectric single crystal other than quartz with stable reproducible properties at room temperatures and good mechanical strength which is readily available in large sizes in commercial quantities. Since the piezoelectric constants of lithium niobate are an order or magnitude larger than those of quartz, lithium niobate should prove useful for a wide variety of stress transducer applications.

The present investigation shows that the three crystallographic orientations of lithium niobate investigated are well suited for current-mode piezoelectric gauges for time-resolved measurements of wave profiles in shock-loaded solids. The effects of electromechanical coupling on current will cause significant nonlinearities in time but these effects can be accounted for by numerical deconvolution techniques.[46,47]

ACKNOWLEDGMENTS

The author is pleased to acknowledge the excellent technical assistance of R. D. Jacobson and review of the manuscript by P. C. Lysne, W. B. Benedick, and L. W. Davison.

APPENDIX: HYDROSTATIC PIEZOELECTRIC CONSTANTS OF LITHIUM NIOBATE OBTAINED FROM DIFFERENT COMMERCIAL SUPPLIERS

In order to further investigate the question of reproducibility of piezoelectric constants of lithium

TABLE VIII. Hydrostatic piezoelectric constants of lithium niobate obtained from various suppliers. ± indicates standard error.

Supplier	d_h (10^{-12} CN^{-1})	d_{hh} (10^{-2} C m^{-2} GPa^{-2})
Crystal Technology Composite (see Ref. 16)	6.31 ± 0.014	0.088 ± 0.0005
Range (five samples, seven experiments)	6.23 to 6.38	0.078 to 0.106
Alpha Company (one sample)	6.34 ± 0.044	0.085 ± 0.005
Harshaw (one sample)	6.34 ± 0.035	0.088 ± 0.004
Isomet (optical grade) (one sample)	6.34 ± 0.017	0.086 ± 0.002
Union Carbide (one sample)	6.39 ± 0.012	0.086 ± 0.001

niobate from sample to sample, the hydrostatic piezoelectric constants of single samples from four additional suppliers, Alpha Co. (Japan), Harshaw, Isomet, and Union Carbide, were determined and compared to the original investigation[16] on five samples from Crystal Technology, Inc. All of the materials of the present investigation were transducer grade except for the material from Isomet which was optical grade. The original investigation of the hydrostatic piezoelectric constants and details of technique are reported in Ref. 16.

Hydrostatic piezoelectric polarization versus pressure data were fit by the relation $P_3^h = d_h p + \frac{1}{2} d_{hh} p^2$, where d_h is the second-order hydrostatic piezoelectric constant and d_{hh} is the third-order hydrostatic piezoelectric constant. The results of the measurements are shown in Table VIII. Although the investigation of materials from each new supplier is limited to single measurements on single samples, the constants determined from the measurements show excellent agreement among the various suppliers. The difference in mean values are well within the expected experimental errors.

*Work supported by the U.S. Energy Research and Development Administration, ERDA, under contract E(29-1)789.

[1]1975 *Ultrasonics Symposium Proceedings*, edited by J. deKlerk (IEEE, New York, 1975).
[2]R.B. Thompson and C.F. Quate, J. Appl. Phys. 42, 907 (1971).
[3]R.A. Graham, F.W. Neilson, and W.B. Benedick, J. Appl. Phys. 36, 1775 (1965).
[4]R.A. Graham and R.D. Jacobson, Appl. Phys. Lett. 23, 584 (1973).
[5]R.A. Graham, J. Appl. Phys. 46, 1901 (1975).
[6]K. Hruska, Czech. J. Phys. B11, 150 (1961).
[7]K. Hruska, IEEE Trans. Sonics Ultrason. SU-18, 1 (1971).
[8]A.I. Korobov and V.E. Lyamov, Sov. Phys.-Solid State 17, 932 (1975).
[9]I.J. Fritz, Ferroelectrics 5, 17 (1973).
[10]R.C. Hanson, K. Helliwel, and C. Schwab, Phys. Rev. B 9, 2649 (1974).
[11]M. Luukkala and J. Surakka, J. Appl. Phys. 43, 2510 (1972).
[12]T.C. Lim, E.A. Kraut, and R.B. Thompson, Appl. Phys. Lett. 20, 127 (1972).
[13]J.J. Gagnepain and R. Besson, in *Physical Acoustics* (Academic, New York, 1975), Vol. XI, p. 245.
[14]R.A. Graham, Phys. Rev. B 6, 4779 (1972).
[15]R.A. Graham, Solid State Commun. 12, 503 (1973).
[16]R.A. Graham, Ferroelectrics 10, 65 (1976).
[17]W.P. Mason, *Piezoelectric Crystals and Their Application to Ultrasonics* (Van Nostrand, New York, 1950), p. 463.
[18]D.H. McMahan, J. Acoust. Soc. Am. 44, 1007 (1968).
[19]P.H. Carr, Phys. Rev. 169, 718 (1968).
[20]A.A. Chaban, JETP Lett. 6, 381 (1967).
[21]S.S. Mathur and P.N. Gupta, Acoustica 23, 160 (1970).
[22]V.E. Ljamov, J. Acoust. Soc. Am. 52, 199 (1972).
[23]P.C. Lysne, J. Appl. Phys. 43, 425 (1972).
[24]Y. Nakagawa, K. Yamanouchi, and K. Shibayama, J. Appl. Phys. 44, 3969 (1973).
[25]R.A. Graham, Proceedings, Microwave Acoustics Symposium, University of Lancaster, 1974 (unpublished).
[26]R.N. Thurston, in *Handbuch der Physik—Encyclopedia of Physics*, edited by S. Flügge and C. Truesdell (Springer-Verlag, New York, 1974). Vol. VIa/4.
[27]E.A. Kraut, T.C. Lim, and B.R. Tittmann, Ferroelectrics 3, 247 (1972).
[28]H.F. Tiersten, Int. J. Eng. Sci. 9, 587 (1971).
[29]W.G. Cady, *Piezoelectricity* (Dover, New York, 1964), Vol. I, p. 196.
[30]J.N. Johnson, J. Appl. Phys. 42, 5522 (1971).
[31]J.N. Johnson (private communication).
[32]P.J. Chen, L. Davison, and M.F. McCarthy, J. Appl. Phys. 47, 4759 (1976).
[33]G.E. Ingram and R.A. Graham, in *Proceedings Fifth Symposium on Detonation*, Office of Naval Research Report ACR-184, 1970, edited by S. Jacobs (U.S. GPO, Washington, D.C. 1970), p. 369.
[34]S. Thunborg, Jr., G.E. Ingram, and R.A. Graham, Rev. Sci. Instrum. 35, 11 (1964).
[35]K.W. Schuler, J.W. Nunziato, and E.K. Walsh, Int. J. Solids Struct. 9, 1237 (1973).
[36]R.A. Graham and W.J. Halpin, J. Appl. Phys. 39, 5077 (1968).
[37]R.A. Graham, J. Phys. Chem. Solids 35, 355 (1974).
[38]The value for Γ for compression along the Z axis was computed according to the formulation of Key [J. Appl. Phys. 38, 2923 (1967)] with elastic and thermal expansion constants reported by Smith and Welsh (Ref. 39) and a specific heat value of 0.635 J/g K. The primary pyroelectric coefficient is computed from the pyroelectric coefficient observed at constant stress p by the relation $\tau = p - e_{33}\alpha_3 - 2e_{31}\alpha_1$ are the linear thermal expansion coefficients. Derivation of the relation between the primary and the constant stress pyroelectric coefficients is given by Glass [J. Appl. Phys. 40, 4699 (1969)] and Thurston (Ref. 26). A value of $p = 7.3 \times 10^{-5}$ C/m^2 K was measured in the present work.
[39]R.T. Smith and F.S. Welsh, J. Appl. Phys. 42, 2219 (1971).
[40]A.W. Warner, M. Onoe, and G.A. Coquin, J. Acoust. Soc. Am. 42, 1223 (1967).
[41]R.W. Smith, Proc. IEEE 59, 712 (1971).
[42]V.V. Chkalova, V.S. Bondarenko, G.O. Fokina, and F.N. Strizhevskaya, Bull. Acad. Sci. USSR, Phys. Ser. 35, 1712 (1971).
[43]A.P. Korolyuk, L.Ya. Matsakov, and V.V. Vasil'chenko, Sov. Phys.-Crystallogr. 15, 893 (1971).
[44]R.A. Graham and G.E. Ingram, J. Appl. Phys. 43, 826 (1972).
[45]R.A. Graham and L.C. Yang, J. Appl. Phys. 46, 5300 (1975).
[46]L.W. Bickle and R.C. Dove, Instrum. Soc. Am. Trans. 12, 286 (1973).
[47]R.P. Reed, Sandia Laboratories Report SC-DC-71 4529, 1971 (unpublished).